Suspended Matter, Chl-a, CDOM, Grain Sizes, and Optical Properties in the Arctic Fjord-Type Estuary, Kangerlussuaq, West Greenland During Summer

Lars Chresten Lund-Hansen ·
Thorbjørn Joest Andersen ·
Morten Holtegaard Nielsen · Morten Pejrup

Abstract Optical constituents as suspended particulate matter (SPM), chlorophyll (Chl-a), colored dissolved organic matter (CDOM), and grain sizes were obtained on a transect in the arctic fjord-type estuary Kangerlussuaq (66°) in August 2007 along with optical properties. These comprised diffuse attenuation coefficient of downwelling PAR (K_d(PAR)), upwelling PAR (K_u(PAR)), particle beam attenuation coefficient (c_p), and irradiance reflectance R (−0, PAR). PAR is white light between 400 and 700 nm. The estuary receives melt water from the Greenland Inland Ice and stations covered a transect from the very high turbid melt water outlet to clear marine waters. Results showed a strong spatial variation with high values as for suspended matter concentrations, CDOM, diffuse attenuation coefficient K_d(PAR), particle beam attenuation coefficients (c_p), and reflectance R(−0, PAR) at the melt water outlet. Values of optical constituents and properties decreased with distance from the melt water outlet to a more or less constant level in central and outer part of the estuary. There was a strong correlation between inorganic suspended matter (SPMI) and diffuse attenuation coefficient K_d(PAR) (r^2=0.92) and also for particle beam attenuation coefficient (c_p; r^2=0.93). The obtained SPMI specific attenuation—K_d^*(PAR)=0.13 m^{2}g^{-1} SPMI—and the SPMI specific particle beam attenuation—c_p^*= 0.72 m^{2}g^{-1}—coefficients were about two times higher than average literature values. Irradiance reflectance R(−0, PAR) was comparatively high (0.09−0.20) and showed a high (r^2=0.80) correlation with K_u(PAR). Scattering dominated relative to absorption—b(PAR)/a(PAR)=12.3. Results strongly indicated that the high values in the optical properties were related to the very fine particle sizes (mean=2–6 μm) of the suspended sediment. Data and results are discussed and compared to similar studies from both temperate and tropical estuaries.

Keywords Fjord-type estuary · Glacio-marine · Suspended matter · PAR attenuation · Particle beam attenuation · Reflectance · Greenland

L. C. Lund-Hansen (✉)
Marine Ecology, Biological Institute, Åarhus University,
Ole Worms Allé 1, Build. 1134, Århus C,
8000 Åarhus, Denmark
e-mail: lund-hansen@biology.au.dk

T. J. Andersen · M. Pejrup
Institute of Geology and Geography, Copenhagen University,
Øster Voldgade 10,
1350 Copenhagen K, Denmark

M. H. Nielsen
Arctic Technology Center, Department of Civil Engineering,
Technical University of Denmark,
Building 204, Kemitorvet,
2800 Kgs. Lyngby, Denmark

Introduction

There are few in situ studies of optical properties from the Arctic regions (e.g., Stramska et al. 2003; Vasseur et al. 2003; Retamal et al. 2007, 2008) in spite of these regions importance in a climate change context (e.g., Lozan et al., 2006). For instance, variations in melt water discharge from inland ice, ice caps, or glaciers will strongly affect turbidity and thereby inherent and apparent optical properties, as well as the light demanding primary

production (Kirk 1994; Retamal et al. 2008). This applies especially for the glacio-marine estuaries and coastal waters which receive the melt water. Optical constituents and properties can serve as proxies for possible changes in melt water discharge, and thus temperature with the positive correlation between run-off and air temperature as observed in West Greenland (Hanna et al. 2008). The in situ optical studies from Arctic regions are fundamental as ground truth data in development of proper remote sensing algorithms (Matsuoka et al. 2007; Drobot 2007).

The Kangerlussuaq in West Greenland receives highly turbid melt water directly from the Greenland Inland Ice during the summer melting period, and the Kangerlussuaq is here characterized as a fjord-type estuary (Perillo 1995). The estuary is very long and narrow and the melt water outlet at the head establishes a gradient from highly turbid waters to very clear open marine waters at the mouth. A cruise was organized in August 2007 in order to study the spatial variation in optical constituents as suspended particulate matter, Chl-a, and colored dissolved organic matter (CDOM) relative to the optical properties as PAR diffuse and particle beam attenuation coefficients, and reflectance. The main questions raised in the present study are: (1) what is the spatial variation in optical constituents? (2) Which optical constituent(s) dominates relative to PAR diffuse and particle beam attenuation coefficients, and reflectance? (3) What are the relations between the optical constituents and the optical properties?

Study Area

The Kangerlussuaq is about 180 km long and the width varies between 5–6 km in the inner part and 1–2 km in the outer part with a total surface area of about 490 km^2 (Fig. 1). The Kangerlussuaq consists of a more shallow (30–40 m) outer part, which connects the open ocean and the inner fjord. The shallow part extends for about 90 km between the ocean and the inner deep water section with water depths up to 280 m in the central part. The tide is diurnal with a tidal range of about 3 m (Nielsen et al. 2010). Melt water from the Greenland Inland Ice enters the estuary mainly through the Watson River (Fig. 1). Average summer discharge is about 120–200 m^3 s^{-1} with suspended matter concentrations of 1,020–1,200 g m^{-3} in the river (Hasholt and Mernild, personal communication). This equals a total suspended matter transport of about 10.757–20.736 tons day^{-1}. A second melt water river enters the fjord south of the Watson River (Fig. 1). The discharge is unknown but assumed to be comparable to the Watson River, as the dimensions (width) of the two rivers are quite similar.

Methods and Materials

CTD, Optical Sensors, and Data Processing

Data were obtained during a 4-day cruise between 6 and 9 August 2007 onboard "Navarana". A total number of 12 stations were covered during the cruise with combined water sampling and optical and CTD casts. A Seabird (SBE 19 Plus) CTD equipped with a Niskin bottle (5 l) for water sampling was applied. Optical data were obtained with optical sensors mounted on a stainless steel frame with a battery pack and data logger (Campbell CR10X). Data on downwelling irradiance—E_d(PAR) (µE m^{-2}s^{-1})—and up-welling irradiance—E_u(PAR) (µE m^{-2}s^{-1})—were obtained by two sensors (Li-192, LICOR), one on top of the frame pointing upwards and one at the bottom of the frame pointing downwards. PAR is the photosynthetic available radiation covering the visible (400–700 nm) part of the spectrum. The E_u(PAR) data were not corrected for self-shading effects (Gordon and Ding 1992) as the E_u(PAR) sensor is placed 20 cm below and lateral of the housing, which has a diameter of 14 cm. Optical measurements were carried out at high solar angles (see later discussion) whereby the effects of self-shading were supposed to be minimal. The diffuse attenuation coefficients K_d(PAR) and K_u(PAR) were derived for each station by means of linear regressions of the log-transformed irradiance data: E_d(PAR) and E_u(PAR). The linear regression model between irradiance and depth described data very well ($r^2 \sim 0.97$) in accordance with: $I = I_0\, e^{-K_d^{(PAR)*z}}$ (Kirk 1994). The irradiance reflectance $R(-0, PAR)$ just below the surface is the ratio between $E_u(-0, PAR)/E_d(-0, PAR)$ (Kirk 1994). Both $E_d(-0, PAR)$ and $E_u(-0, PAR)$ were estimated by a linear regression of the log-transformed E_d(PAR) and E_u(PAR) to derive $E_d(-0, PAR)$ and $E_u(-0, PAR)$ at the surface (-0), following the method by Pfannkuche (2002). The linear regressions only comprised data obtained between surface and 2−3 m of water depth to minimize the effects of the differences in the spectral composition of E_u(PAR) and E_d(PAR). Waters were calm without any waves affecting optical measurements. The Fig. 2 shows typical profiles of E_d(PAR) and E_u(PAR) (station C). All optical casts, except for one, were carried out at solar elevations higher than 27° to have a sufficiently strong underwater irradiance penetration (Davies-Colley et al. 1993). A Wetlabs C-Star transmissometer at an operating wavelength of 660 nm (red light) measured light transmission across a path length of 0.25 m. The particle beam attenuation coefficient related to particles (c_p) was derived as: $c_p - c_w = \ln(T_r)/r$ where T_r is the transmittance, r the path length, and c_w the light attenuation coefficient in pure water (Smith and Baker 1981). Absorption by CDOM was assumed to be negligible at 660 nm (Jerlov 1976). All data including depth (pressure) and temperature were stored on

Fig. 1 Study area with the location of the Kangerlussuaq Fjord in West Greenland and the different stations
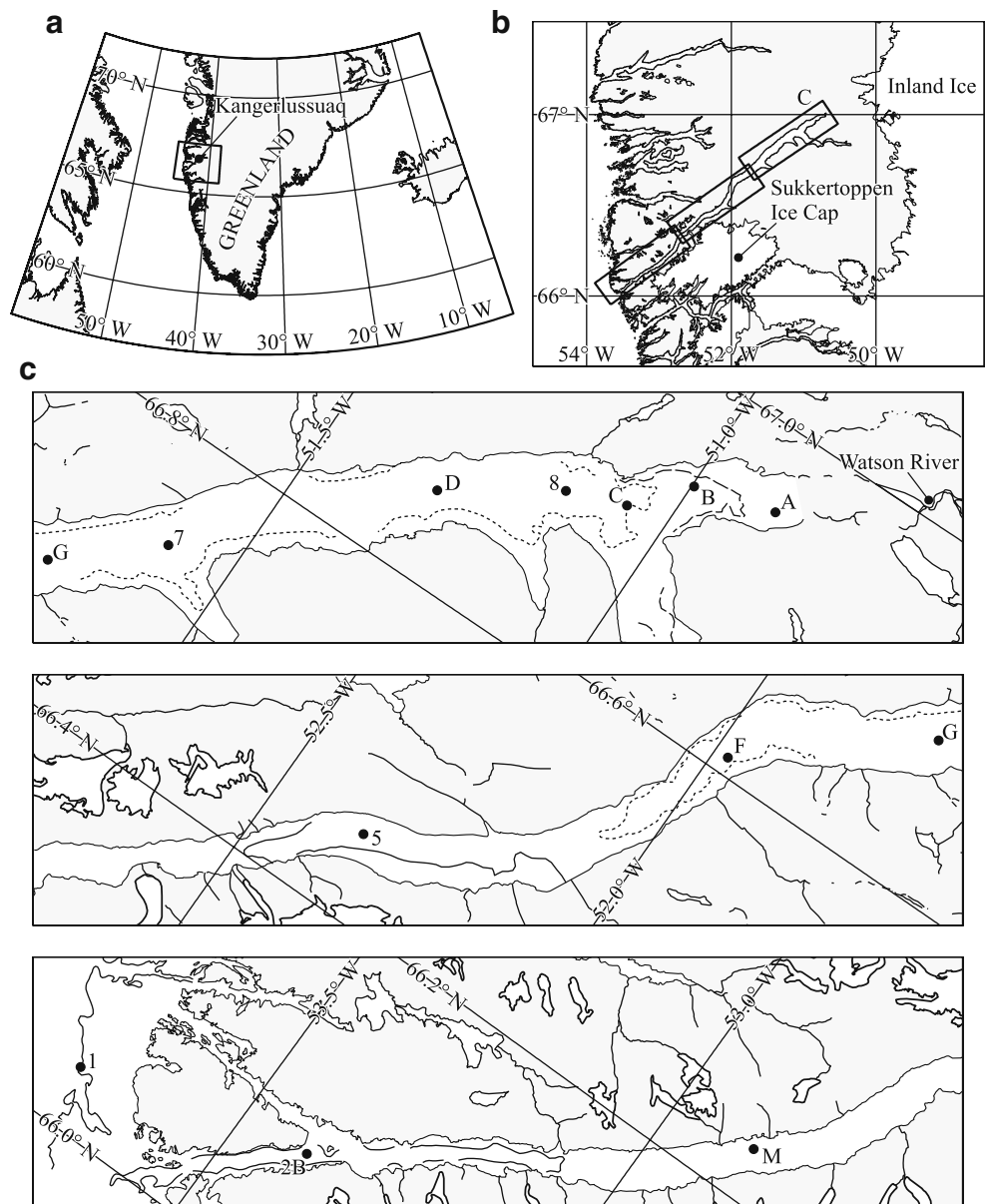
the data logger placed in the steel casing. Variables were measured to a depth of about 30–35 m with a vertical resolution of 0.1 m with a descend velocity of the optical sensor package of about 0.1 ms^{-1}. Weather conditions were sunny with a few clouds. Optical casts were carried out on sunny side of the ship to avoid any effects of the shadow from the ship. Average cosine μ_0, the angles the photons make with the vertical in the water, was calculated for each cast according to time, date, and latitude using standard nautical handbooks.

Chl-a, Suspended Matter, and CDOM

An exact volume (0.5–1 l) of water was filtered through glass fiber filters (GF75 Advantec) with a nominal size

of 0.3 μm, using a vacuum of maximally 30 kPa (0.3 bar). The filters were packed individually in tin-foil bags and stored in a household freezer at −18°C. In laboratory filters were stored in 5-ml 96% ethanol at 5°C for a minimum of 6 and a maximum of 20 h for pigment extraction from the retained phytoplankton. Samples were centrifuged and the absorbance of the supernatant was measured at 665 and 750 nm with a spectrophotometer (Thermo Spectronic HELIOS λ) and converted into Chl-a concentrations following Strickland and Parsons (1972). Suspended matter concentrations (SPM) were determined by filtration of an exact volume (0.5–1 l) of water through pre-combusted (400°C, 6 h) glass fiber filters (GF/F Whatman) with a nominal pore size of 0.7 μm. Distilled water was used to remove any salt
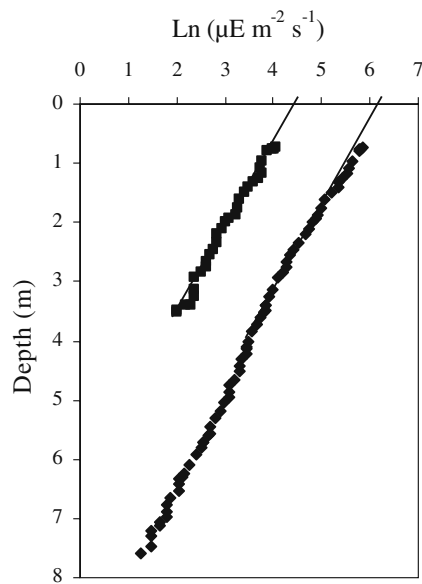
Fig. 2 Downwelling E_d(PAR) and upwelling E_u(PAR) shown as ln (μE m^{-2}s^{-1}) as a function of depth (m) at station C

residues from the filters after filtration of the sample. The filters were kept dark and cold until arrival in laboratory where they were dried (60°C, 16 h) and weighed. Afterwards, filters were burned (500°C, 16 h), cooled, and weighed to derive organic (SPMO) and inorganic (SPMI) content of the suspended matter (Bowers and Mitchelson-Jacob 1996). SPMT is the concentration of total suspended particulate matter (g m^{-3}), and SPMI is the inorganic part: SPMT=SPMI+SPMO, and SPMO the organic part. Water samples for absorption coefficients of colored dissolved organic matter were pre-filtered onboard using GF75 (Advantec) filters and stored cold and dark in amber-colored 250-ml glass containers. Samples were again filtered in laboratory using 0.2 μm membrane filters, and measured spectrophotometrically (Thermo Spectronic HELIOS λ) by a scanning of the interval 250–750 μm using distilled particle free Millipore water as baseline. Samples were analyzed about 2 weeks after completing the cruise. The absorption coefficient at 440 nm was taken as proportional to CDOM concentrations (Kirk 1994) by:

$$g440 = 2.303(A_{440} - A_{750})/L \qquad (1)$$

where A_{440} and A_{750} are the absorbencies at 440 and 750 nm. L is cuvette path length (0.1 m) and 2.303 converts the base of the logarithm from 10 to e. The SPM concentrations, CDOM absorption coefficients, and Chl-a concentrations were determined for water samples collected at 1 m depth. Note that Chl-a concentrations could not be obtained at stations A, B, C, D, and M due to unfortunate laboratory errors (see later discussion).

Grain Sizes

A volume of 2 l of water was filtered onto 0.45 μm Millipore CEM filters following the sampling. In laboratory, the filters were dispersed with 0.01 M $Na_2P_4O_7$ and sonified for 2 min with a Branson Sonifier 250 in order to destroy all aggregates. The particle size distribution of a sample was obtained with a Malvern Mastersizer 2000 laser diffraction analyser, which has a measurement range of 0.02–2,000 μm (http://www.malvern.com). This is the particle size distribution of the primary grains suspended in the water but measured in the laboratory (see later discussion). The in situ particle size distribution was obtained with a LISST 100 particle sizer with a working range of 2.5–500 μm (Agrawal and Pottsmith 1994). The LISST 100 was lowered to a depth of about 30 m with a descent velocity of about 0.1 ms^{-1}.

Results

SPMT, Chl-a CDOM, Salinity, and Temperature

Total suspended particulate matter (SPMT) concentrations of the surface water (1 m depth) were high near the melt water outlet at stations A (372.7 gm^{-3}) and B (123.3 gm^{-3}), and decreased to an average concentration of 3.6 gm^{-3} for remaining stations. SPMT concentration was 2.3 gm^{-3} at the outermost marine station (Fig. 3a). The organic matter content of SPMT determined by loss of ignition was low at stations A and B (1.3–2.2%), higher between stations C and 2b (16.4%), and 55% at station 1 outside the estuary. All data are listed in Table 1. There was only a small spatial variation in Chl-a along the transect with an average concentration of 1.17 mg Chl-a m^{-3} (Fig. 3c). The CDOM absorption coefficients varied between 0.046 and 0.36 (m^{-1}) with high values (~0.23 m^{-1}) at the melt water outlet and low (~0.07 m^{-1}) values at all other stations (Fig. 3c). Surface salinity was fairly constant around 5 PSU in the inner half of the estuary from where it gradually increased to 29 PSU outside (Fig. 3d). Temperature increased gradually in the inner part from 3.5°C at the melt water outlet to 8°C around station 5 due to solar heating whereas mixing of water masses at shallow (~50 m) water at 90 km reduced temperature and increased salinity (Fig. 3d).

K_d(PAR), c_p, and R(−0, PAR)

Diffuse attenuation coefficient K_d(PAR) decreased from very high values (15.34–6.57 m^{-1}) at stations A and B near the melt water outlet to 0.12 m^{-1} at the entrance of the estuary (Fig. 3b). Raised K_d(PAR) values at stations 5 and M relate to the Sarfatoq River, which discharges into the

Fig. 3 a Total suspended matter concentrations SPMT (g m^{-3}) and particle beam attenuation coefficient c_p (m^{-1}) at stations along the transect from the river outlet (A–B) to the marine station (1); **b** diffuse attenuation coefficient K_d(PAR) (m^{-1}); **c** Chl-a concentrations (mg Chl-a m^{-3}) and CDOM absorption coefficients (m^{-1}); **d** salinity (PSU) and temperature (°C)
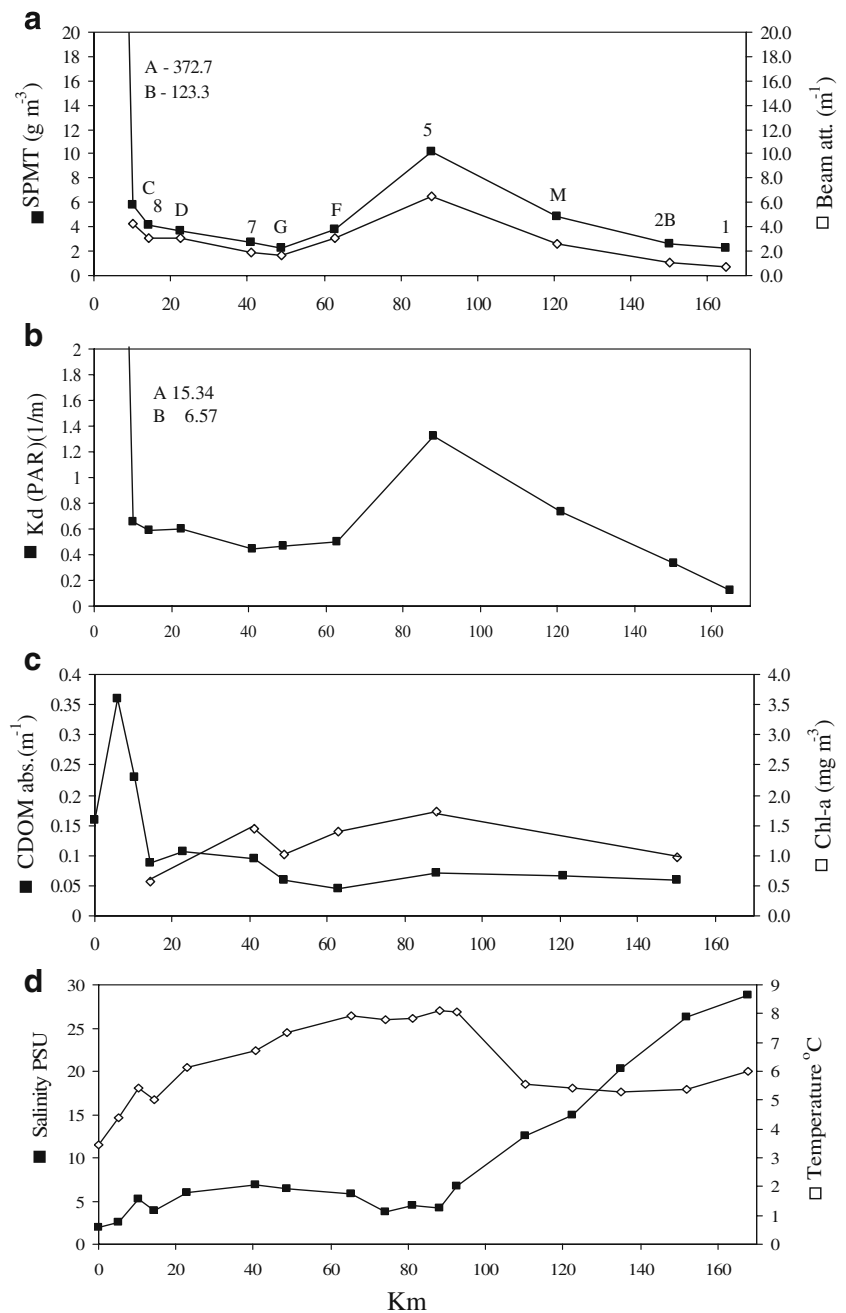
Kangerlussuaq near station 5 (Fig. 1). The presence of the Sarfatoq River was also recognized by the raised SPMT concentrations (Fig. 3a). The spatial distribution of K_d(PAR) equalled the SPMT distribution (Fig. 3a, b), as shown by the high ($r^2=0.92$) and positive correlation between SPMI and K_d(PAR) (Fig. 4a). The equation of the regression line between SPMI and K_d(PAR) reads: $y=0.13\times$SPMI$+0.1$. The coefficient of 0.13 is the SPMI-specific attenuation coefficient K^*_d(PAR) (m^{2}g^{-1} SPMI) and 0.1 (m^{-1}) is K_d(PAR) in the SPMI depleted water mass. The 0.1 equalled K_d(PAR)=0.12 at the marine station 1, where SPMI concentrations were low (1.5 g m^{-3}) (Table 1).

The outlier data point ($x=1.45$; $y=0.12$) in Fig. 4a is the marine station 1 outside the estuary (Fig. 1).

The particle beam attenuation coefficient (c_p) varied between 6.45 and 0.7 (m^{-1}) with a maximum at station 5 and a minimum at station 1 outside the fjord (Fig. 3b). Note that a c_p could not be obtained at stations A and B as SPMT concentrations (372.3–123.3 g m^{-3}) exceeded the measuring range of the transmissometer. However, spatial distributions of c_p and SPMT concentrations were very similar (Fig. 3a), as demonstrated by the strong ($r^2=0.93$) and positive correlation between SPMI and c_p (Fig. 4b). The equation of the regression line reads: $y=0.72\times$SPMI$+0.2$, where

Table 1 Station number, SPMT (total; g m^{-3}), SPMI (inorganic; g m^{-3}), SPMO (percent), K_d(PAR) (m^{-1}), irradiance reflectance $R(-0, \text{PAR})$, particle beam attenuation coefficient (c_p; m^{-1}), CDOM (m^{-1}) Chl-a (mg m^{-3}), salinity (PSU), temperature (°C), and μ_0 average cosine

Sta.	SPMT (gm^{-3})	SPMI (gm^{-3})	SPMO (%)	K_d(PAR) (m^{-1})	$R(-0, \text{PAR})$	Beam (m^{-1})	CDOM (m^{-1})	Chl-a (mgm^{-3})	Salt	Temp. (°C)	μ_0
A	372.3	367.7	1.3	15.34			0.159		1.44	3.43	0.80
B	123.3	120.7	2.2	6.57			0.359		2.56	4.37	0.82
C	5.8	5.2	11.5	0.65	0.16	4.24	0.230		5.17	5.42	0.82
8	4.1	3.6	13.9	0.60	0.20	3.10	0.087	0.56	3.87	5.03	0.82
D	3.7	3.2	15.6	0.60	0.19	3.09	0.106		5.94	6.13	0.77
7	2.7	2.1	32.2	0.45	0.10	1.90	0.094	1.44	6.82	5.70	0.71
G	2.3	1.9	21.0	0.47	0.09	1.71	0.059	1.02	6.37	7.35	0.82
F	3.7	3.4	11.9	0.50	0.14	3.10	0.046	1.44	5.82	7.81	0.80
5	10.1	9.0	12.3	1.32	0.15	6.45		1.72	4.17	8.10	0.77
M	4.9	4.4	12.6	0.73	0.15	2.55	0.071		14.70	5.41	0.74
2B	2.6	1.9	37.8	0.34	0.10	1.11	0.067	0.96	26.34	5.36	0.69
1	2.3	1.5	55.2	0.12		0.71	0.059		28.86	6.00	

0.72 is the SPMI-specific particle beam attenuation coefficient (c_p*) (m^{2}g^{-1} SPMI; Fig. 4b). The ordinate intercept of 0.2 deviates from the theoretically 0.0 but the discrepancy might attribute to a low number of observations in such SPMI particle beam attenuation correlations (Campbell and Spinrad 1987).

The irradiance reflectance $R(-0, \text{PAR})$ varied between a maximum of 0.20 at station 8 and a minimum of 0.09 at station G with an average of 0.14. Irradiance reflectance $R(-0, \text{PAR})$ distribution in the estuary resembled those of K_d(PAR), c_p, and SPMT (Fig. 3a, b) with high values in inner part of the estuary and lower in the outer (Table 1). A plot of K_u(PAR) against $R(-0, \text{PAR})$ shows a high correlation ($r^2 = 0.80$) except for two outlier points (stations 5 and M), which are excluded from the regression (Fig. 4c). The equation of the regression line reads: $R(-0, \text{PAR}) = 0.26 K_u(\text{PAR}) + 0.0$ where the coefficient 0.26 (m) express a degree of reflectance. It shows that an increase in diffuse attenuation of the upwelling PAR—K_u(PAR)—gives a higher reflectance—$R(-0, \text{PAR})$—at the surface. All correlation coefficients between parameters are listed in the correlation matrix (Table 2).

In Situ Grain Sizes and Primary Particles

The particle size distributions of primary particles at station B and M are very fine grained with mean particle sizes of 6.0 μm (B) and 2.0 μm (M; Fig. 5a). Very fine-grained (8.7 μm) primary particles were also obtained at station A (not shown). Twenty-two percent of the sample at station B has particle sizes <2 μm, which increased to 43% at station M. Units on abscissa is frequency in terms of volume percent of the sample in each particle size class (Fig. 5a). Note that these primary particle size distribu-

tions were measured in the laboratory (see "Methods and Materials").

The in situ particle size distributions were obtained with the LISST instrument between 0 and 1 m depth (see "Methods and Materials"), and results from station C showed a particle size distribution with a mode at about 30 μm and a mean particle size about 22 μm (Fig. 5b). Data from each particle size interval are the average of 12 measurements shown with the standard deviation and frequency as volume percent as in Fig. 5a. About 18% of the material in the sample is <8.0 μm, but note that data are truncated at the lower limit (2.5 μm) of the instrument measuring range whereby actual content of the particles <8.0 μm might be >18%. The differences in particle sizes between LISST in situ (Fig. 5b) and the primary particles (Fig. 5a) are caused by flocculation of the primary particles in the water. The primary particles are flocculated due to differences in electrical charge between clay particles (negative) and the cations (positive) in the saltwater (Eisma 1993; Hill et al. 2000). Mean particle size of the in situ flocculated particles was 56.0 μm (station B), 22.0 μm (station C), 39.0 μm (station 8), and 140.0 μm (station 1). It is estimated that more than 60% of a total sample is flocculated by analyzing the relative distributions of a combined primary particle and an in situ particle size distribution.

Discussion

The Optical Constituents: SPM, Chl-a, and CDOM

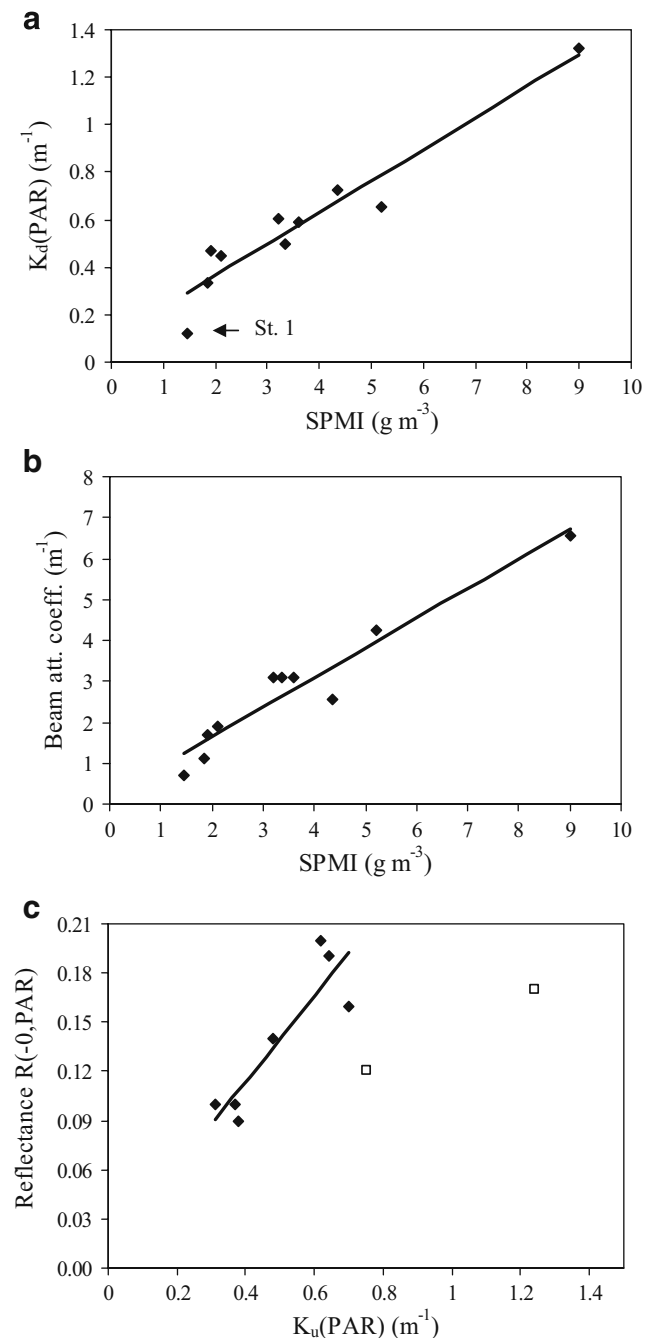Optical constituents and properties were measured at 12 stations along the transect (Fig. 1). It could be argued that

Fig. 4 a The relation between inorganic SPMI (g m^{-3}) and diffuse attenuation coefficient K_d(PAR) (m^{-1}); **b** the relation between inorganic SPMI (g m^{-3}) and particle beam attenuation coefficient c_p (m^{-1}); **c** the relation between K_u(PAR) (m^{-1}) and $R(-0$, PAR)

the numbers of stations are limited. The strategy was sampling at high spatial resolution where SPM gradients, for instance, were assumed to be steep and a lower resolution where the gradient was low. Results showed, in fact, high values in optical constituents and properties at the melt water outlet and more or less constant values in central and outer part. It is strongly supposed that the main elements regarding optical constituents and properties in

the estuary during summer are comprised in the present study.

The high SPMT concentrations near the melt water outlet at stations A (372.7 gm^{-3}) and B (123.3 gm^{-3}) are similar to those in tropical estuaries as the Mekong River (~250 gm^{-3}) (Wolanski et al. 1996) and the Red River, also Vietnam, at low flow concentrations (~200 gm^{-3}; van Maren and Hoekstra 2004). The low (2.0–4.0 gm^{-3}) SPMT concentrations in the outer part of the estuary are comparable to those in the estuarine North Sea–Baltic Sea transition (Lund-Hansen 2004; Lund-Hansen and Christiansen 2008). The low concentrations are also comparable to dry period SMPT concentrations in the tropical Nha Phu estuary (Lund-Hansen et al. 2010). The Chl-a concentrations 1–1.5 mg Chl-a m^{-3} are similar to spring (May) concentrations (0.8–1.5 mg Chl-a m^{-3}) in the arctic Disko Bay, West Greenland, (Heide-Jørgensen et al. 2007).

The spatial distribution and values of CDOM coefficient in Kangerlussuaq are very similar to those obtained in the tropical Nha Phu estuary (Lund-Hansen et al. 2010). They both showed high values (0.2–0.3 m^{-1}) near the fresh water source, i.e., the melt water in Kangerlussuaq and the river in Nha Phu, and lower (0.05–0.1 m^{-1}) values in outer part of the estuaries. The high (0.2–0.3 m^{-1}) CDOM coefficients are comparable to those obtained in the estuarine North Sea–Baltic Sea transition (Lund-Hansen 2004). CDOM originates from degradation of organic material of terrestrial origin and ends up in the marine environment via the rivers (Kirk 1994). It is interesting that CDOM coefficients are very similar in three very different estuarine environments. There were no relations between salinity and CDOM coefficients (r^2=0.19) in the Kangerlussuaq as often observed in terms of a negative correlation in freshwater influenced fjords and estuaries (Bowers et al. 2004; Shank et al. 2009; Lund-Hansen et al. 2010). A reason might be the absence of a gradual mixing of the freshwater and saltwater in inner part of the estuary (~0–90 km; Fig. 3d).

The Optical Properties: K_d(PAR), c_p, and $R(-0$, PAR)

There was a considerable range between the very high (15.34 m^{-1}) K_d(PAR) at station A at the melt water outlet and the K_d(PAR) of 0.12 m^{-1} at station 1 in the outer marine part of the estuary (Table 1). However, the K_d(PAR) range in the main part of the estuary of 0.12–0.79 m^{-1} equaled observations (0.15–0.56 m^{-1}) from the estuarine North Sea–Baltic Sea transition (Lund-Hansen 2004), a range of New Zealand estuaries (0.3–1.1 m^{-1}; Vant 1990), a NZ coastal site (0.067–0.78; Pfannkuche 2002), and outer part of the tropical Nha Phu (~0.25 m^{-1}) in dry conditions (Lund-Hansen et al. 2010). An average K_d(PAR) of 0.19 m^{-1} was measured in the arctic Baffin Bay (77° N; Vasseur et al. 2003) and is comparable to present results.

Table 2 Correlation matrix: diffuse attenuation coefficients $K_d(PAR)$ (m^{-1}), $K_u(PAR)$ (m^{-1}), particle beam attenuation coefficient (c_p; m^{-1}), SPMT (total; g m^{-3}), SPMI (inorganic; g m^{-3}), Chl-a (mg m^{-3}), CDOM absorption coefficient (m^{-1}), $R(-0, PAR)$

	$K_d(PAR)$	$K_u(PAR)$	Beam att.	SPMT	SPMI	Chl-a	CDOM	$R(-0, PAR)$
$K_d(PAR)$	*							
$K_u(PAR)$	0.96	*						
Beam att.	0.87	0.87	*					
SPMT	0.89	0.94	0.90	*				
SPMI	0.92	0.95	0.93	0.99	*			
Chl-a	0.30	0.23	0.30	0.07	0.08	*		
CDOM	0.0	0.0	0.08	0.42	0.46	0.02	*	
$R(-0, PAR)$	0.48	0.80	0.56	0.14	0.45	0.0	0.15	*

There was a very high ($r^2 = 0.92$) correlation between SPMI concentrations and $K_d(PAR)$ with a SPMI-specific attenuation coefficient $K^*_d(PAR)$ of 0.13 m^{2}g^{-1} SPMI (Fig. 4a). This value was high as compared to published values: 0.07 m^{2}g^{-1} SPM (Christian and Sheng 2003), 0.06 m^{2}g^{-1} SPM (Pfannkuche 2002), and 0.1 m^{2}g^{-1} SPM (McMahon et al. 1992). These values comprise both marine and more turbid estuarine environments and demonstrates that $K^*_d(PAR)$ in the Kangerlussuaq was about two times higher than average for comparable SPMI concentrations.

Particle beam attenuation coefficient (c_p) showed a wide range between 0.71 and 6.45 m^{-1} (Fig. 3b; Table 1), which is similar to that obtained at an oceanic to coastal water gradient in the Gulf of Mexico (Gould and Arnone 1997), and also similar to the range observed in nine NZ estuaries (1.3–5.2 m^{-1}; Vant 1990). The present specific SPMT particle beam attenuation coefficient (c_p^*) of 0.80 m^{2}g^{-1} SPMT was about two times higher as compared to literature values from different turbid estuaries: 0.44 m^{2}g^{-1} SPM (Krause and Ohm 1984), 0.4 m^{2}g^{-1} SPM (Vant 1990), and 0.55 m^{2}g^{-1} SPM (Wells and Kim 1991). There is a record of a similar (0.81 m^{2}g^{-1} SPM) and high specific attenuation coefficient from the Lena River entering the Kara Sea (Vasilkov et al. 1999). Particle beam attenuation depends, apart from the concentration, on size, shape, and refractive index of the particles in suspension (Kirk 1994). Baker and Lavelle (1984) showed a clear inverse correlation between particle size diameter and specific SPM particle beam attenuation coefficient, as (c_p^*) increased with a decrease in particle sizes. Several field studies have also shown a higher particle beam attenuation at more fine-grained suspensions but for similar mass concentrations (Moody et al. 1987; Wiberg et al. 1994; Bunt et al. 1999).

Irradiance reflectance was generally high in the Kangerlussuaq with a range of 0.09–0.20 as compared to the $R(-0, PAR)$ ranges (0.056–0.12) in nine New Zealand estuaries (Vant 1990) and NZ coastal areas (0.014–0.12; Pfannkuche 2002) with similar SPM concentrations as in the present study. A $R(-0) = 0.2$ have been observed in the Rhone River plume (Ouillon et al. 1997).

Reflectance is caused by scattering of the light by particles in the water (Kirk 1994) and Pfannkuche's (2002) relations for absorption—a(PAR)—and scattering coefficients—b(PAR)—were applied to validate that scattering dominated relative to absorption. This shows that a(PAR)=0.13 m^{-1} and b(PAR)=1.61 m^{-1} for average SPMT, CDOM, and Chl-a concentrations comprising stations C to 1, and gives a scattering/absorption ratio: b(PAR)/a(PAR)=12.3. It demonstrates a high scattering as compared to data from an estuarine–coastal environment for comparable CDOM absorption, Chl-a, and SPMT concentrations (Pfannkuche 2002). The high scattering in the Kangerlussuaq was strongly supposed to be dominated by SPMT, as compared to the foremost absorbers: Chl-a and CDOM, as these
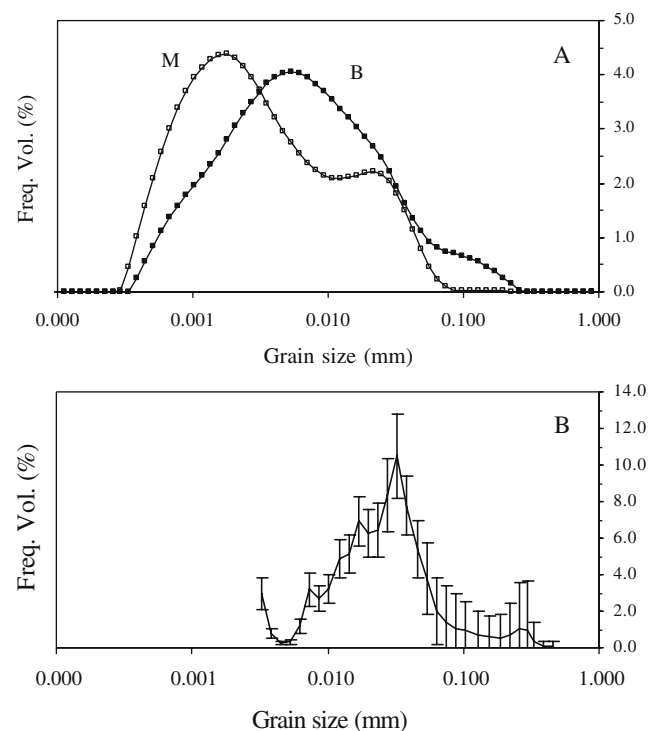

Fig. 5 a Particle size distribution of the primary particles at stations M and B; **b** in situ particle size distribution of flocculated material between 0 and 1 m at station C

occurred at low concentrations (Chl-a~1.0 mg m^{-3}) and low absorption coefficients (CDOM~0.1 m^{-1}; Table 1).

Particle Sizes

Optical properties of the SPM are dominated by the size, shape, and refractive index of the SPM (Kirk 1994). Only the SPM particle sizes were studied here in more detail as particle sizes are the main variables considering the negative correlation between particle sizes and particle beam attenuation coefficient (Baker and Lavelle 1984). The particle sizes of the primary particles (2–6 μm) were clearly more fine grained as compared to other arctic marine and estuarine environments as Howe Sound, British Columbia (Syvitski and Murray 1981), McBeth Fiord, Baffin Island (Winters and Syvitski 1992), Disenchantment Bay, Alaska (Curran et al. 2004), and the Kuannersuit Sulluat Fjord, West Greenland (Sulsbrück 2007), which generally showed mean particle sizes around 5–10 μm. The average of the mean flocculated particle size in Kangerlussuaq was 64 μm for stations B, C, 8, and 1, which was comparatively low. Other LISST in situ flocculated particles reached 120–150 μm (Bowers et al. 2007) at Menai Bridge, Wales, an average of 66.5 μm (39–109 μm) in the Danish Sound (Mikkelsen and Pejrup 2000), and an average of 210 μm (32–442 μm) from various estuarine and coastal sites (Mikkelsen et al. 2005). Flocculated particle size varied between 50 and 200 μm in the Mekong River though determined with another method (Wolanski et al 1996). However, these particle sizes are more comparable to those from the present marine station 1 (140 μm). It is thus strongly supposed that the high SPMI-specific particle beam and diffuse attenuation coefficients were actually related to the very fine-grained SPM in accordance with these results. The very fine-grained particles in suspension in the water with a low settling velocity (~0.02 mm s^{-1}) were supposedly derived as glacial flour and transported to the estuary with the melt water (Andersen et al. 2010). Nevertheless, the results from the present work clearly call for further studies of the relations between grain sizes and optical properties.

References

Andersen, T.J., Nielsen, M.H., Lund-Hansen, L.C., Hasholt, B. and M. Pejrup. 2010. Low-density flocs in an Arctic fjord, Kangerlussuaq, West Greenland. Estuarine, Coastal, and Shelf Science (Submitted).

Agrawal, Y., and H.C. Pottsmith. 1994. Laser diffraction particle sizing in STRESS. Continental Shelf Research 14: 1101–1121.

Baker, J.W., and E.T. Lavelle. 1984. The effect of particle size on the light attenuation coefficient of natural suspensions. Journal of Geophysical Research 89(C5): 8197–8203.

Bowers, D.G., and E.G. Mitchelson-Jacob. 1996. Inherent optical properties of the Irish Sea determined from underwater irradiance measurements. Estuarine, Coastal and Shelf Science 43: 433–447.

Bowers, D.G., D. Evans, D.N. Thomas, K. Ellis, and P.J. Williams. 2004. Interpreting the colours of an estuary. Estuarine, Coastal, and Shelf Science 59: 13–20.

Bowers, D.G., C.E. Binding, and K.M. Ellis. 2007. Satellite remote sending of the geographical distribution of suspended particle size in an energetic shelf area. Estuarine, Coastal, and Shelf Science 73: 457–466.

Bunt, J.A.C., P. Larcombe, and C.F. Jago. 1999. Quantifying the response of optical backscatter devices and transmissometers to variations in suspended particulate matter. Continental Shelf Research 19: 1199–1220.

Campbell, D.E., and R.W. Spinrad. 1987. The relationship between light attenuation and particle characteristics in a turbid estuary. Estuarine, Coastal, and Shelf Science 25: 53–65.

Christian, D., and Y.P. Sheng. 2003. Relative influence of various water quality parameters on light attenuation in Indian River Lagoon. Estuarine, Coastal and Shelf Science 57: 961–971.

Curran, K.J., P.S. Hill, T.G. Milligan, E.A. Cowan, J.P.M. Syvitski, and S.M. Konings. 2004. Fine-grained sediment flocculation below the Hubbard Glacier melt water plume, Disenchantment Bay, Alaska. Marine Geology 203: 83–94.

Davies-Colley, R.J., W.N. Vant, and D.G. Smith. 1993. Colours and clarity of natural waters: Science and management of optical water quality. New York: Ellis Horwood.

Drobot, S.D. 2007. Using remote sensing data to develop seasonal outlooks for Arctic regional sea-ice minimum extent. Remote Sensing of Environment 222: 136–147.

Eisma, D. 1993. Suspended Matter in the Aquatic Environment. Berlin: Springer. 315 pp.

Gordon, H., and K. Ding. 1992. Self-shading of in-water optical instruments. Limnology and Oceanography 37: 491–500.

Gould, R.W., and R.A. Arnone. 1997. Estimating the beam attenuation coefficient in coastal waters from AVHRR imagery. Continental Shelf Research 17: 1375–1387.

Hanna, E., P. Huybrechts, K. Steffen, J. Cappelen, R. Huff, C. Shuman, I.-F. Tristram, S. Wise, and M. Griffiths. 2008. Increased runoff from melt from the Greenland Ice sheet: A response to global warming. Journal of Climate 15: 331–341.

Heide-Jørgensen, M.P., K.L. Laidre, M.L. Logsdon, and T.G. Nielsen. 2007. Springtime coupling between chlorophyll-a, sea ice, and sea surface temperature in Disko Bay, West Greenland. Progress in Oceanography 73: 79–97.

Hill, P.S., T.G. Milligan, and W.R. Geyer. 2000. Controls on the effective settling velocity of suspended sediments in the Eel river flood plume. Continental Shelf Research 20: 2095–2111.

Jerlov, N.G. 1976. Marine Optics, 2nd ed. Elsevier Oceanography Series, 14. Amsterdam, 371 pp.

Kirk, J.T.O. 1994. Light and Photosynthesis in the aquatic ecosystems. Cambridge University Press, 509 pp.

Krause, G., and K. Ohm. 1984. A method to measure suspended load transports in estuaries. Estuarine, Coastal and Shelf Science 19: 611–618.

Lozan, J.L., Grassl, H., Hubberten, H.-W., Hupfer, P., Karbe, L., and D. Piepenburg. (eds.). 2006. Warming signals from polar regions—Scientific facts. Wissenshaftliche Auswertungen, Hamburg, Germany, 351 pp.

Lund-Hansen, L.C. 2004. Diffuse attenuation coefficients K$_d$(PAR) at the estuarine North Sea-Baltic Sea transition: Time-series,

partitioning, absorption, and scattering. *Estuarine, Coastal, and Shelf Science* 61: 251–259.

Lund-Hansen, L.C., and C. Christiansen. 2008. Suspended particulate matter (SPM) in the North Sea-Baltic Sea transition: Ditributions, inventories, and the autumn 2002 inflows. *Danish Journal of Geography* 108: 37–47.

Lund-Hansen, L.C., Hai, Lam, N.N. and M.H. Nielsen. 2010. Optical properties of a tropical estuary during wet and dry conditions in the Nha Phu estuary, Khan Hoa Province, south-east Vietnam. *Hydrobiologia*, 644: 207–216.

van Maren, D.S., and P. Hoekstra. 2004. Seasonal variation of hydrodynamics and sediment dynamics in a shallow subtropical estuary: The Ba Lat River, Vietnam. *Estuarine, Coastal and Shelf Science* 60: 529–540.

Matsuoka, A., Y. Huot, and K. Shimada. 2007. Bio-Optical characteristics of the western Arctic Ocean: Implications for ocean colour algorithms. *Canadian Journal of Remote Sensing* 33: 503–518.

McMahon, T.G., R.C.T. Raine, T. Fast, L. Kies, and J.W. Patching. 1992. Phytoplankton biomass, light attenuation and mixing in the Shannon Estuary, Ireland. *Journal of Marine Biological Association UK* 72: 709–720.

Mikkelsen, O.A., and M. Pejrup. 2000. In situ particle size spectra and density of particle aggregates in a dredging plume. *Marine Geology* 170: 443–459.

Mikkelsen, O.A., P.S. Hill, T.G. Milligan, and R.J. Chant. 2005. In situ particle size distribution and volume concentrations from a LISST-100 laser particle sizer and a digital floc camera. *Continental Shelf Research* 25: 1959–1978.

Moody, J.A., B. Butman, and M.H. Bothner. 1987. Near-bottom suspended matter concentration on the continental shelf during storms: Estimates based on in situ observations of light transmission and a particle size dependent transmissometer calibration. *Continental Shelf Research* 7: 609–628.

Nielsen, M.N., Reng, D., and K.L. Knudsen. 2010. Physical oceanographic conditions and recent foraminefera in Kangerlussuaq. *Polar Research* (In press).

Ouillon, S., P. Forget, J.M. Froidefond, and J.J. Naudin. 1997. Estimating suspended matter concentrations from SPOT data and from field measurements in the Rhone river plume. *Journal of Marine Technology Society* 31: 15–20.

Pfannkuche, J. 2002. Optical properties of Otago shelf waters: South Island New Zealand. *Estuarine, Coastal, and Shelf Science* 55: 613–627.

Perillo, G.M.E. 1995. *Geomorphology and sedimentology of Estuaries*. Amsterdam: Elsevier. 471 pp.

Retamal, L., W.F. Vincent, C. Martineau, and C.L. Osburn. 2007. Comparison of the optical properties of dissolved organic matter in two river-influenced coastal regions of the Canadian Arctic. *Estuarine, Coastal, and Shelf Science* 72: 261–272.

Retamal, L., S. Bonilla, and W.F. Vincent. 2008. Optical gradients and phytoplankton production in the Mackenzie River and the coastal Beaufort Sea. *Polar Biology* 31: 363–379.

Shank, G.C., K. Nelson, and P.A. Montagna. 2009. Importance of CDOM distribution and photoreactivity in a shallow Texas estuary. *Estuaries and Coasts* 32: 661–677.

Smith, R.C., and K.S. Baker. 1981. Optical properties of the clearest natural waters (200–800 nm). *Applied Optics* 37: 2216–2227.

Stramska, M., D. Stramski, R. Hapter, S. Kaczmarek, and J. Ston. 2003. Bio-optical relationsships and ocean algorithms for the north polar region of the Atlantic. *Journal of Geophysical Research. C. Oceans* 108: C5.

Strickland, J.D.H., and T.R. Parsons. 1972. *A practical Handbook of Seawater Analyses*. Canada: Ottawa. 239 pp.

Sulsbrück, H. 2007. From clay to climate. Sediment processes and Holocene sedimentary fjord environments, West Greenland. Unpublished Phd thesis, University of Copenhagen

Syvitski, J.M., and J.W. Murray. 1981. Particle interaction in fjord suspended sediment. *Marine Geology* 39: 215–242.

Vant, W.N. 1990. Causes of light attenuation in nine New Zealand estuaries. *Estuarine, Coastal, and Shelf Science* 31: 125–137.

Vasilkov, A.P., V.I. Burenkov, and K.G. Ruddicj. 1999. The spectral reflectance and transparency of river plume waters. *International Journal of Remote Sensing* 20: 2497–2508.

Vasseur, C., B. Mostajir, C. Nozais, M. Denis, E. Fouilland, B. Klein, and S. Demers. 2003. effects of bio-optical factors on the attenuation of ultraviolet and photosynthetically available radiation in the North water Polynya. *Marine Ecology Progress Series* 252: 1–13.

Wiberg, P.L., D.E. Drake, and D.A. Cachione. 1994. Sediment resuspension and bed armouring during high bottom stress events on the northern California inner continental shelf: Measurements and predictions. *Continental Shelf Research* 14: 1191–1219.

Winters, G.V., and J.P.M. Syvitski. 1992. Suspended sediment character and distribution in McBeth Fjord, Baffin Island. *Arctic* 45: 25–35.

Wolanski, E., N.H. Nguyen, L.T. Dao, N.H. Nhan, and N.N. Thuy. 1996. Fine-sediment dynamics in the Mekong River Estuary, Vietnam. *Estuarine, Coastal and Shelf Science* 43: 565–582.

Wells, J.T., and S.-Y. Kim. 1991. The relationship between beam transmission and concentration of suspended particulate material in the Neuse River estuary, North Carolina. *Estuaries* 14: 395–403.